Examination of the Three-Dimensional Geometry of Cetacean Flukes Using Computed Tomography Scans: Hydrodynamic Implications

FRANK E. FISH,[1]* JOHN T. BENESKI,[1] AND DARLENE R. KETTEN[2]
[1]Department of Biology, West Chester University, West Chester, Pennsylvania
[2]Department of Biology, Woods Hole Oceanographic Institution, Woods Hole, Massachusetts

ABSTRACT

The flukes of cetaceans function in the hydrodynamic generation of forces for thrust, stability, and maneuverability. The three-dimensional geometry of flukes is associated with production of lift and drag. Data on fluke geometry were collected from 19 cetacean specimens representing eight odontocete genera (*Delphinus*, *Globicephala*, *Grampus*, *Kogia*, *Lagenorhynchus*, *Phocoena*, *Stenella*, *Tursiops*). Flukes were imaged as 1 mm thickness cross-sections using X-ray computer-assisted tomography. Fluke shapes were characterized quantitatively by dimensions of the chord, maximum thickness, and position of maximum thickness from the leading edge. Sections were symmetrical about the chordline and had a rounded leading edge and highly tapered trailing edge. The thickness ratio (maximum thickness/chord) among species increased from insertion on the tailstock to a maximum at 20% of span and then decreasing steadily to the tip. Thickness ratio ranged from 0.139 to 0.232. These low values indicate reduced drag while moving at high speed. The position of maximum thickness from the leading edge remained constant over the fluke span at an average for all species of 0.285 chord. The displacement of the maximum thickness reduces the tendency of the flow to separate from the fluke surface, potentially affecting stall patterns. Similarly, the relatively large leading edge radius allows greater lift generation and delays stall. Computational analysis of fluke profiles at 50% of span showed that flukes were generally comparable or better for lift generation than engineered foils. *Tursiops* had the highest lift coefficients, which were superior to engineered foils by 12–19%. Variation in the structure of cetacean flukes reflects different hydrodynamic characteristics that could influence swimming performance. Anat Rec, 290:614–623, 2007.

Key words: Cetacea; cross-sectional geometry; morphology; chord; thickness ratio; leading edge radius; odontocete; *Delphinus*; *Globicephala*; *Grampus*; *Kogia*; *Lagenorhynchus*; *Phocoena*; *Stenella*; *Tursiops*; NACA0012; NACA0021

Grant sponsor: ONR; Grant number: N00014-02-1-0046.

*Correspondence to: Frank E. Fish, Department of Biology, West Chester University, West Chester, PA 19383.
E-mail: ffish@wcupa.edu

Received 2 March 2007; Accepted 6 March 2007
DOI 10.1002/ar.20546
Published online in Wiley InterScience (www.interscience.wiley.com).

The morphological design of organisms affects their locomotor performance. The external shape of the body is in intimate contact with the environmental medium. Animals that move through water must contend with momentum transfer in a highly dense fluid. Such constraints place severe selection pressures on body shape to facilitate economical and efficient movement in water, particularly at high speed. The similarity that fish display in body design and propulsive mode with cetaceans is considered a prime example of evolutionary convergence (Howell, 1930). Such convergence is associated with constraints imposed on animals by the physical environment and with selection for morphological, physiological, and behavioral adaptations for swimming that maximizes energy economy and thrust production (Daniel and Webb, 1987; Schultz and Webb, 2002).

Members of the order Cetacea (i.e., whales, dolphins, porpoises) are characterized as high-speed swimmers (Lang and Daybell, 1963; Fish and Rohr, 1999; Rohr et al., 2002) possessing both flukes and flippers (see Cooper et al., 2007, this issue, on cetacean flipper anatomy). The propulsive structures of cetaceans are the flukes. The flukes are lateral extensions of the distal tail. Structurally, the flukes are composed of fibrous connective tissue (Felts, 1966). Biomechanically, the flukes act like a pair of wings (Vogel, 1994). Thrust is generated as a component of an anteriorly directed lift force as the flukes are vertically oscillated (Fish, 1998a,b). Despite the importance of the flukes as the sole propulsive device, there has been limited research into the anatomical design of these structures.

Felts (1966) and Purves (1969) described the composition of the soft tissue anatomy of the flukes. The flukes are composed of a cutaneous layer, a subcutaneous blubber layer, a ligamentous layer, and a core of dense fibrous tissue. The bulk of the fibrous tissue is composed of collagen fibers, which are arranged in horizontal, vertical, and oblique bundles.

Data were presented on the geometry of the flukes for various species of cetaceans (Lang, 1966; Purves, 1969; van Oosanen and Oosterveld, 1989; Bose and Lien, 1989; Bose et al., 1990; Fish, 1998b; Fish and Rohr, 1999). Cross-sectional profiles of the flukes along the longitudinal axis display a conventional streamlined foil profile with a rounded leading edge and long tapering trailing edge. This shape is crucial for generation of lift for thrust, while minimizing drag (Lighthill, 1970; Vogel, 1994). The flukes are symmetrical about the chord (Lang, 1966; Bose et al., 1990).

The cross-sectional profile of the flukes is similar to symmetrical engineered foils (Fish, 1998b). The resemblance to engineered foils suggests that the flukes would be able to produce high lift with low drag at high angles of attack. This performance would be possible because the shape of the fluke section would permit water flow to move cleanly over its surface. In addition, the symmetrical design of the fluke profiles indicates that thrust is generated on both up- and down-strokes (Fish, 1993, 1998a).

This study provides a detailed quantitative description of the geometry of cetacean flukes. By using CT scans (computer assisted tomography), finely detailed geometric data can be collected without damage to the specimen. The data can be reassembled digitally to determine the three-dimensional geometry of a complex structure (Fig. 1). In addition, the digitized geometry can be used in computational aero- and hydrodynamic models to assess performance associated with morphology. The flukes of various species are compared to identify morphological differences and determine levels of hydrodynamic performance, based on the specific geometry of fluke profiles.

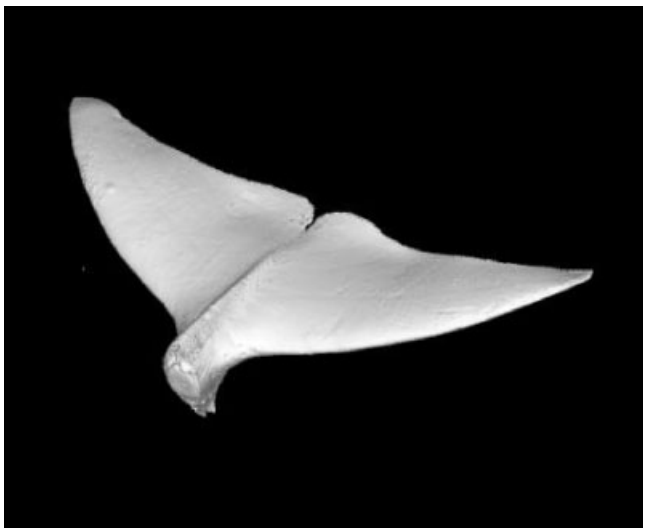

Fig. 1. Three-dimensional reconstruction of dolphin fluke from sequential 1-mm computed tomography scans.

MATERIALS AND METHODS

The flukes from 19 cetacean specimens representing eight odontocete genera were obtained from dead stranded animals collected by the New Jersey Marine Mammal Stranding Center (Brigantine, NJ). Species included one common dolphin (*Delphinus delphis*), one long-finned pilot whale (*Globicephala melaena*), two Risso's dolphins (*Grampus griseus*), two pygmy sperm whales (*Kogia breviceps*), two Atlantic white-sided dolphins (*Lagenorhynchus acutus*), seven harbor porpoises (*Phocoena phocoena*), one spotted dolphin (*Stenella* sp.), and three bottlenose dolphins (*Tursiops truncatus*).

Animals were transported to the University of Pennsylvania School of Veterinary Medicine, New Bolton Center for necropsy. Flukes were removed from the carcass, sealed in plastic bags, and subsequently frozen at 19°C and stored at West Chester University. Flukes remained frozen as they were transported to Woods Hole Oceanographic Institution for CT scanning. The flukes were thawed before scanning. Flukes were laid flat on the scanner table, using plastic wedges and Styrofoam sheets for support. Flukes were oriented dorsal side up and scanned in the spanwise direction from fluke tip to tip. This orientation permitted images of cross-sections to be analyzed directly.

CT scans were obtained on a Siemens Volume Zoom CT scanner at the Woods Hole Oceanographic Institution Ocean Imaging Center. Spiral protocols for data acquisition with 0.5- to 1-mm detector collimation at 1 mm/sec table feeds were used. All images were reconstructed in two formats (i.e., using conventional soft tissue and

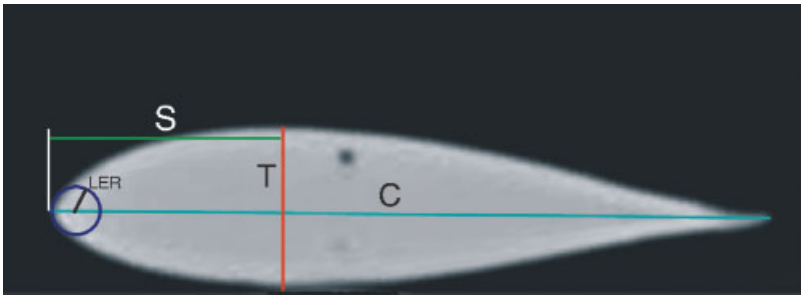

Fig. 2. Cross-section dimensions of fluke computed tomography image. The light blue line (*C*) is the chordline, the red line is the maximum thickness (*T*), and the green line is the distance to the maximum thickness from the leading edge (shoulder, *S*). The black line is the leading edge radius (*LER*), which is determined from radius of the blue circle that connects tangency points of the leading edge with the upper and lower surfaces of the cross-section.

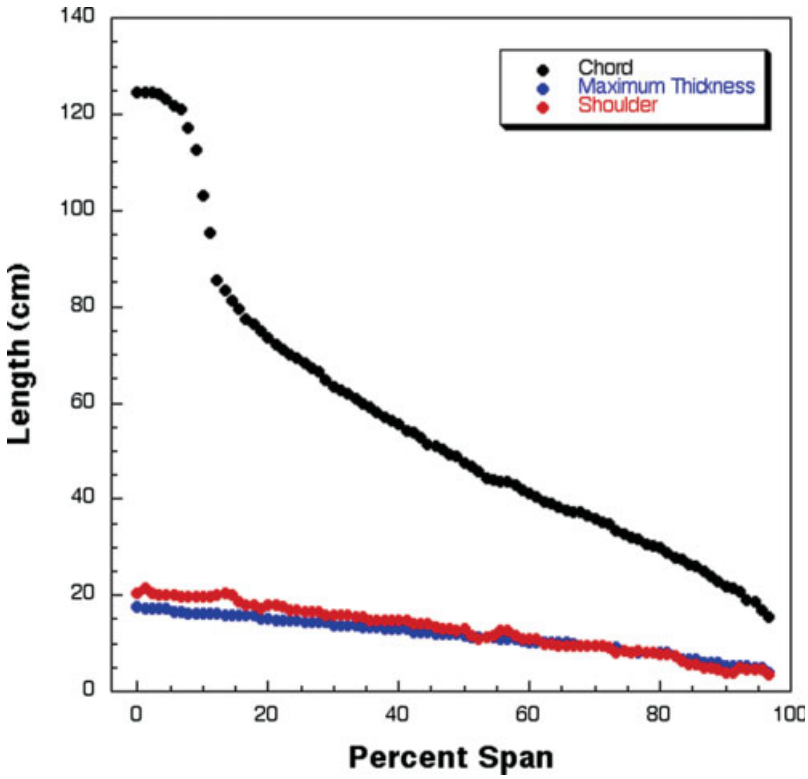

Fig. 3. Linear measurements of the *Stenella* sp. fluke showing changes in the chord (*C*), maximum thickness, and the shoulder (*S*).

ultra-high kernels). Image reformats were provided as 512 matrix DICOM outputs. A 10-fold expansion of the attenuation scale was applied to the data to improve discrimination of higher density components of structural elements as well as to eliminate artifacts from any potential metallic inclusions in the tissues. Images, in some instances, were reconstructed at 100-μ slice intervals to provide data-based enhancements of the tissues under investigation. With these parameters, the maximum in-plane resolution was 0.35 mm at 2% of the modulation transfer function. This provided image data sets with isotropic 100 μ/side voxels. Prior studies suggest 25 μ in-plane pixel resolutions are possible, but a conservative nominal resolution is 50 μ.

Raw attenuation data were archived onto both CD and magneto-optical disks for all scans. Raw data were stored as a 1,024 × 1,024 attenuation matrix coded in 4,096 levels of attenuation. Image files were produced in 512 × 512 matrices with attenuations compressed and represented visually as a 256 gray scale. Enlargements of image files are "empty magnifications"; therefore, retaining raw attenuation data allows data-based magnifications for maximum visual information. Images were also archived on disk and printed as conventional CT films.

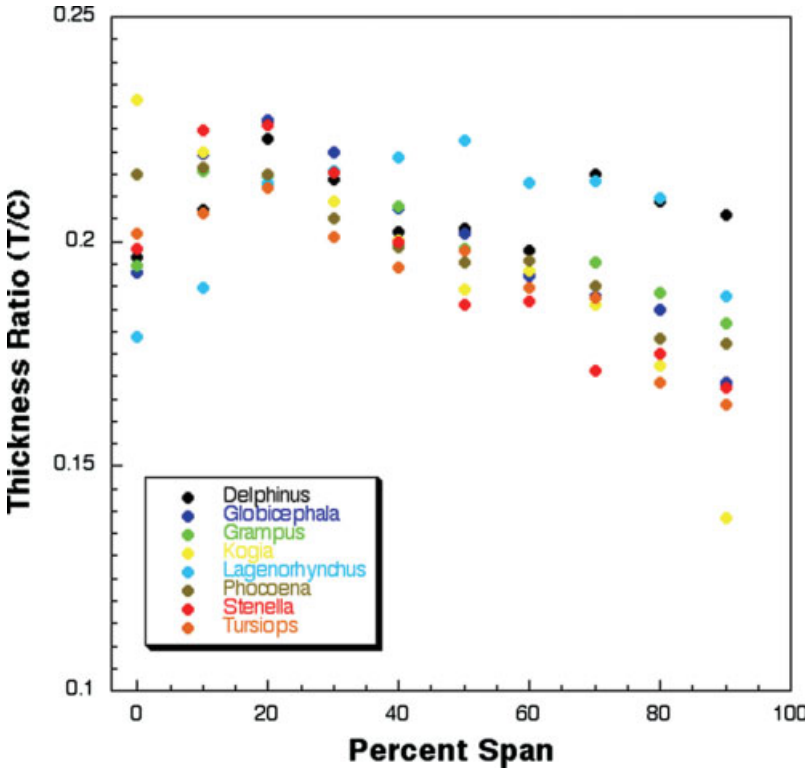

Fig. 4. Distribution of thickness ratio (*TR*) over the span of the fluke.

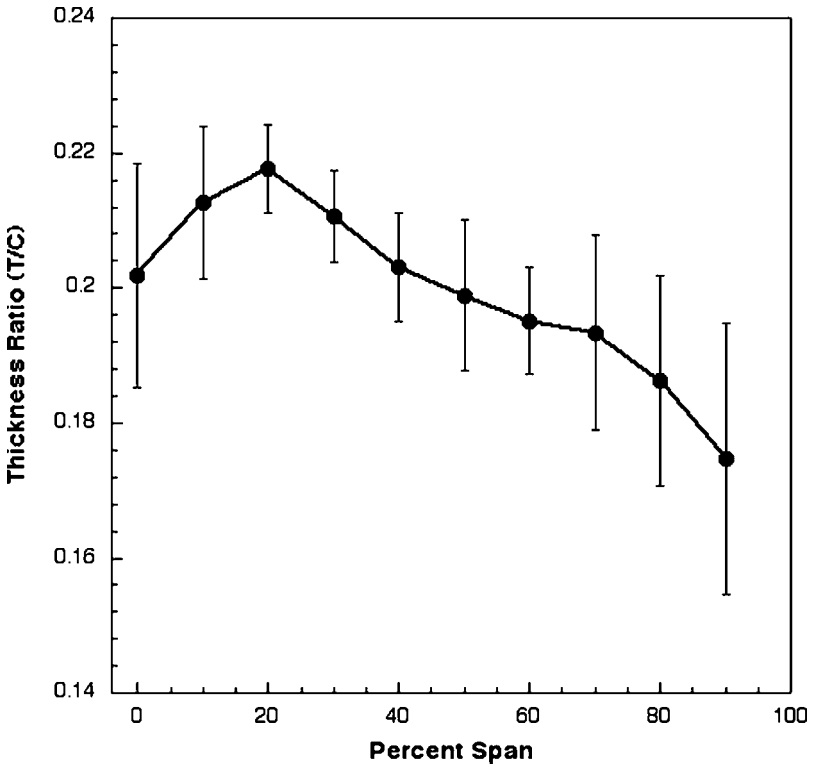

Fig. 5. Mean±SD of thickness ratio (*TR*) over the span of the fluke. Maximum thickness occurs at 20%. Fluke thickness decreases regularly toward the tip.

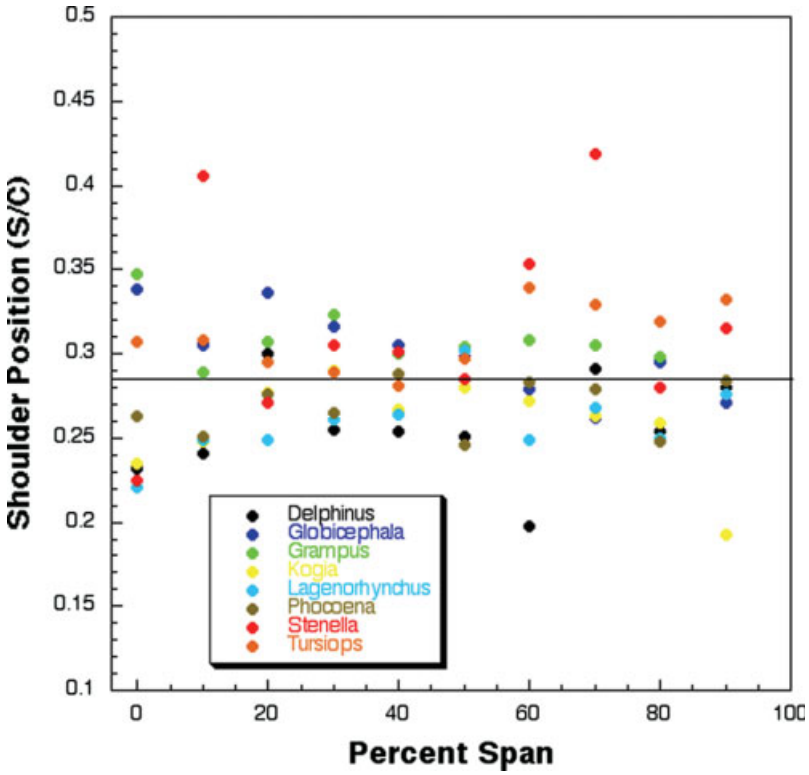

Fig. 6. Plot of the shoulder position (*SP*) as a function of the percent of span. The solid line indicates mean *SP* for the pooled sample of all species.

TABLE 1. Leading edge radius for eight species of cetaceans

Species	Leading edge radius (mean ± SD)
Delphinus delphis	0.034
Globicephala melaena	0.039
Grampus griseus	0.037 ± 0.001
Kogia breviceps	0.046 ± 0.007
Lagenorhynchus acutus	0.038 ± 0.001
Phocoena phocoena	0.041 ± 0.007
Stenella sp.	0.032
Tursiops truncatus	0.035 ± 0.004

DICOM images of fluke cross-sections were analyzed using ImageJ software (NIH version 1.3). Measurements were made along the span of a single fluke from each specimen; the span is the distance from the insertion of the fluke on the tailstock to the fluke tip. Dimensions of the fluke cross-sectional profiles included chord length, maximum thickness, shoulder, and leading edge radius (Fig. 2). The fluke chord (C) was measured as the centerline distance from the leading to trailing edges of the flukes. The maximum thickness (T) was measured as maximum vertical distance between upper and lower surfaces of the flukes. The shoulder (S) was measured as the distance of T from the leading edge. The radius of curvature of the leading edge (*LER*) is the radius of a circle that connects tangency points of the leading edge with the upper and lower surfaces of the cross-section (Hurt, 1965). The center of the circle is a point on the chord line for a symmetrical foil. A circle template was used on images of fluke cross-sections to determine radius of the leading edge, as animals were of different sizes, comparisons of morphology were made using ratios. The thickness ratio ($TR = T/C$) and shoulder position ($SP = S/C$) indicate hydrodynamic performance relating to the generation of lift and drag for foil sections (von Mises, 1945; Hoerner, 1965). *LER* (leading edge radius) was presented also as a proportion of C.

Due to differences in numbers of individuals per species and size of flukes for each species, comparisons were made using means (±SD). Comparisons among species were made at intervals of 10% of fluke span from the insertion of the fluke on the tailstock (0%) to the position at 90% of span toward the tip.

Lift coefficients (C_L) of fluke profiles were calculated using an Airfoil Analysis v1.0.2 (RLM Software). The analysis is an inviscid panel method. Calculations were performed on the digital coordinates for the surface geometry of cross-sections at 50% of fluke span. Lift coefficients were computed for fluke profiles at angles of attack of 5 degrees and 10 degrees. Lift coefficients for fluke profiles were compared with standard aerodynamic symmetrical foil sections (NACA 0012, NACA 0021). As there are accurate data for lift coefficients of these engineered foils, they served as standards to evaluate the lift performance of the fluke profiles and could be used to validate the Airfoil Analysis program.

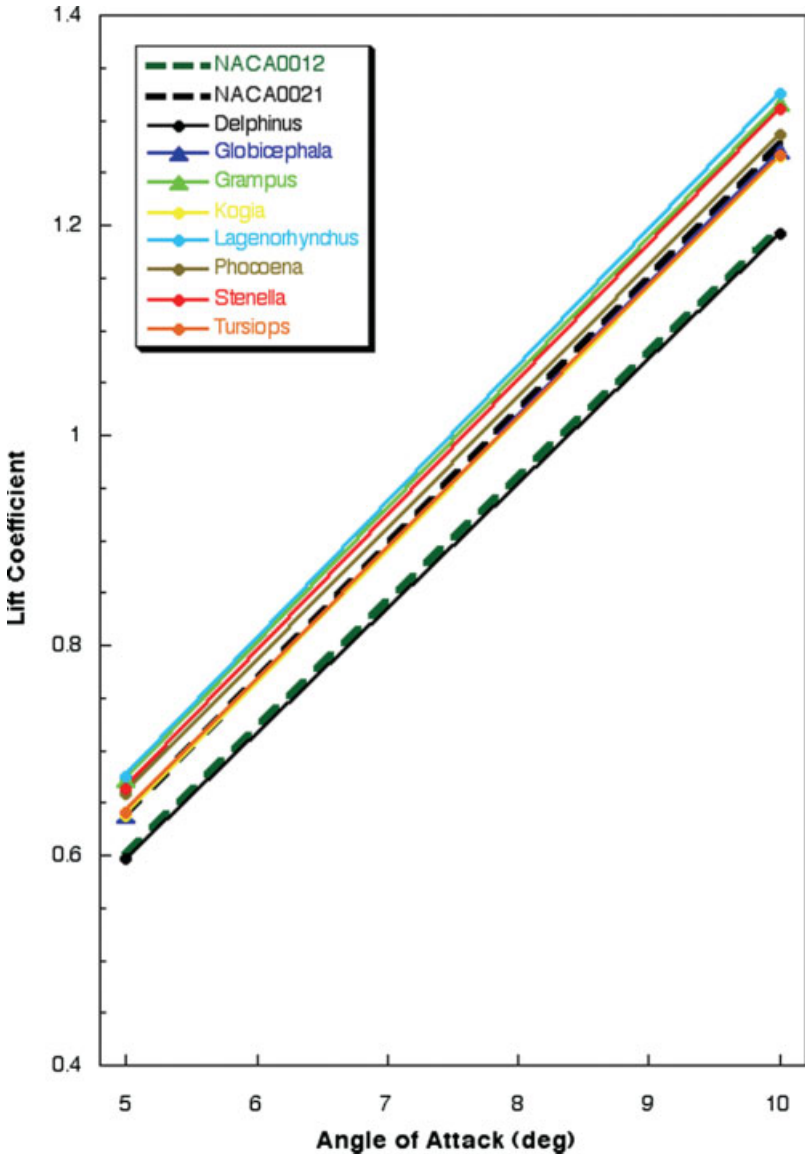

Fig. 7. Comparison of lift coefficients (C_L) among species and standard engineered foils at angles of attack of 5 degrees and 10 degrees.

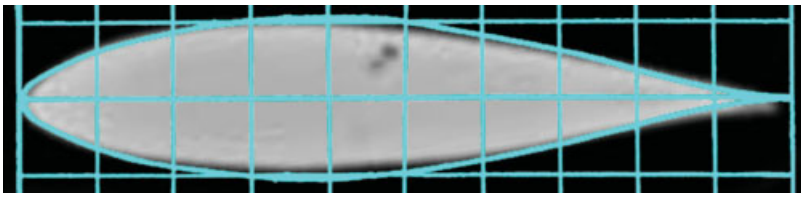

Fig. 8. Overlay of NACA 63-021 foil from Abbott and von Doenhoff (1949) in blue on fluke section for *Stenella* sp. The fluke section has approximately the same outline as the NACA foil.

RESULTS

In cross-section, the flukes displayed a blunt and rounded leading edge and a thin, tapering trailing edge. Cross-sectional profiles were symmetrical about the chord (Fig. 2). Chord (C), maximum thickness (T), and maximum thickness position (S) showed a nonuniform decrease distally (Fig. 3). C was largest close to the tailstock for approximately the first 10% of the span. It is also in this region where C shows the largest decrease.

TABLE 2. Lift coefficient at 10° angle of attack and swimming speeds

Species	C_L (10°)	Maximum (m s^{-1})	Cruise (m s^{-1})	Reference
Delphinus delphis	1.16	12.5–13.9	1.6–2.8	2,5,14
Globicephala melaena	1.27	11.3	2.6–3.6	6,12
Grampus griseus	1.32	7.8–8.9	1.7–1.9	7
Kogia breviceps	1.26	N/A	1.5	10
Lagenorhynchus acutus	1.33	7.7[a]	1.4–3.4	3,8
Phocoena phocoena	1.29	4.6–6.2	1.3–2.0	3,4
Stenella sp.	1.31	6.1–8.2	3.3–4.6	1,11
Tursiops truncatus	1.34	8.2–11.1	2.2–4.2	9,13,15

[a]Value for related species *Lagenorhynchus obliquidens*.
References: 1) Au et al., 1988; 2) Cummings et al., 1968; 3) Curren et al., 1994; 4) Gaskin et al., 1975; 5) Hui et al., 1987; 6) Johanessen and Harder, 1960; 7) Kruse et al., 1999; 8) Lockyer and Morris, 1987; 9) Mörzer Bruyns, 1971; 10) Nowak, 1991; 11) Pilleri and Knuckey, 1969; 12) Rohr et al., 2002; 13) Tomlin, 1957; 14) Wood, 1998.

Beyond this proximal region, *C* decreased steadily toward the tip. Both *S* and *T* decreased at a relatively steady rate from the tailstock to the tip.

The thickness ratio (*TR*) varied along the span of the fluke and among species (Fig. 4). When the data were pooled for all species, *TR* was shown to increase from the tailstock to a maximum at 20% of span. From this point, *TR* decreased steadily to the tip (Fig. 5). The mean *TR* at 20% of span was 0.218 ± 0.007. The maximum value of *TR* was 0.227 for *Globicephala* at 20% of span and the minimum *TR* was 0.139 for *Kogia* near the fluke tip at 90% of span.

The shoulder position (*SP*) remained constant across the span (Fig. 6). Mean SP for the pooled data over the span for all species was 0.285 ± 0.036. The largest mean *SP* over the span was 0.316 ± 0.060 for *Stenella*, and the lowest mean *SP* was 0.256 ± 0.030 for *Delphinus*. *SP* ranged from 0.418 for *Stenella* to 0.193 *Kogia* at 70% and 90% of span, respectively. Spanwise variation was indicated by coefficient of variation (V; Simpson et al., 1960). The smallest V (3.00) occurred at 20% of span; whereas, 90% of span had the largest V (11.46). The *LER* ranged from 0.032 for *Stenella* to 0.041 for *Phocoena* (Table 1).

Lift coefficient increased with angle of attack. *Lagenorhynchus* and *Delphinus* exhibited the largest and smallest C_L, respectively, at angles of attack of 5 degrees and 10 degrees (Fig. 7). Only *Delphinus* had values of C_L below those for the NACA 0012 foil by approximately 0.4%. C_L for *Lagenorhynchus* was 10.8–12.5% greater than for the NACA 0012. Compared with the NACA0021, lower values of C_L were found for *Delphinus*, *Globicephala*, *Kogia*, and *Tursiops* (Fig. 7). The C_L values for *Delphinus* were 7.1% lower than C_L for the NACA 0021 at 10 degrees; whereas, C_L was up to 5.7% higher for *Lagenorhynchus* at 5 degrees.

DISCUSSION

The flukes of modern cetaceans are the primary propulsive structure (Fish and Rohr, 1999). The propulsive motions of the flukes are a combination dorsoventral oscillation (heave) and angular change to the axis of progression of the animal (pitch). In this way, the flukes act as an oscillating wing; whereby, the pitch controls the angle of attack (i.e., angle of fluke longitudinal axis to the incident water flow) so that the flukes generate an anteriorly directed lift force. Thrust is generated as a component of hydrodynamically derived lift over the stroke cycle. Thrust from lift increases directly with angle of attack until stall is reached. Stall is the abrupt loss of lift due typically from separation of flow about the leading edge of a wing or hydrofoil.

As wing-like structures, the flukes can be analyzed like engineered air- and hydrofoils to determine their effectiveness in lift generation (Lang, 1966; Bose et al., 1990; Fish and Battle, 1995; Pavlov, 2003). Well-performing flukes should possess a morphology that maximizes the ratio of lift to drag (i.e., resistive force), generated by their action (Webb, 1975). Therefore, the shape of the flukes influences the energy requirements for swimming. The symmetrical cross-sections of the flukes were highly streamlined and indicate hydrodynamic adaptations for high lift generation. A streamlined shape is characterized by a blunt, rounded leading edge, maximum thickness located one third to one half of the chord posterior of the leading edge, and tapering toward the trailing edge. The rounded leading edge, position of the shoulder, and sharp trailing edge is crucial for lift generation, while minimizing drag (Webb, 1975; Vogel, 1994).

The values of *SP* and *TR* in this study corresponded to previously published values. Fluke sections ranged from 0.25 to 0.4 for *SP* and between 0.16 and 0.25 for *TR* (Lang, 1966; Shpet, 1975; Bose et al., 1990). *SP* and *TR* indicate hydrodynamic performance relating to the generation of lift and drag for the sections of the fluke (von Mises, 1945; Hoerner, 1965). These parameters affect the pressure distribution. A favorable pressure gradient has pressure decreasing in the downstream direction, which facilitates flow over the surface of the fluke. An adverse pressure gradient has pressure increasing in the downstream direction and retards flow over the surface of the fluke. The favorable and adverse pressure gradients are located upstream and downstream of *SP*, respectively. The adverse pressure gradient facilitates flow separation from the fluke surface and results in a large increase in drag (Webb, 1975; Vogel, 1994). By displacement of *SP* further downstream on the fluke section, separation can be delayed by promoting a longer favorable pressure gradient.

Engineered "laminar" foils have a far posteriorly displaced *SP* (0.45) to delay separation and reduce drag (Vogel, 1981; Pavlov, 2003). Researchers believe that more posterior *SP* is associated with faster swimming whales (Shpet, 1975). However, the mean *SP* for all species and sections was only 0.285. The fast swimming dolphins *Stenella* and *Lagenorhynchus* had *SP* values above and below the mean *SP*. This position is most likely a compromise between drag reduction and lift generation at high angles of attack. Although incurring low drag when closely oriented to the on-coming flow, "laminar" foils are prone to turbulence and premature separation with increasing angle of attack (Vogel, 1981). An *SP* that is located along the first third of the chord may be a compromise for flukes. Flukes must maintain lift without stalling while oscillating over a range of angles of attack and simultaneously minimize drag.

Streamlined foil sections with low *TR* have lower drags than high *TR* foils. Low *TR* foils have a small pressure gradient magnitude, which reduces drag. Lift, however, is enhanced and stall delayed as *TR* increases. The NACA 63-006 foil with a *TR* of 0.06 has a lift coefficient approximately 0.87 and a stall angle of 11 degrees, whereas the NACA 63-021 with a *TR* of 0.21 has a lift coefficient approximately 1.40 and a stall angle of 17 degrees (Abbott and von Doenhoff, 1949). The implications for flukes are that inboard portions of the span would generate more lift and be less likely to stall than near the tips. Tip stall may be mitigated by spanwise flexibility. *Lagenorhynchus acutus* displayed a 13% deflection from tip to tip across the fluke span (Curren et al., 1994). The center of the flukes is more rigid than the tips. During the up-strokes fluke tips are bent down slightly from the plane of the fluke and lag behind the center, whereas bending in the opposite direction occurs during the down-stroke. Bose et al. (1990) suggested that the phase difference due to this spanwise flexibility would prevent the total loss of thrust at the end of the stroke. While the tips would be ending the stroke and effectively generating no thrust, the center would have started the next stroke and begin thrust generation.

The range of *LER* measured in this study overlapped the range of values (0.01–0.09) for the flukes of other cetaceans collected by Bose et al. (1990). For both studies, *LER* was higher than engineered airfoils. Airfoils have typical *LER* values of zero (knife edge) to 0.02 (Hurt, 1965). Thick foil shapes (i.e., high *TR*) with large *LER* have higher coefficients of lift than with small *LER* values of 0–0.01 (Jacobs et al., 1933). Increased drag due to a large *LER* is offset by the reduced likelihood of flow separation and stall with increasing angle of attack (Vogel, 1994). Flow can more smoothly move around the leading edge without incurring a large pressure gradient (Lang, 1966). For cetaceans, which oscillate their flukes, a high *LER* would help to avoid separated flow and loss of lift. There would be a smooth transition as the flow reverses direction around the leading edge through the stroke cycle.

The cross-sectional profile of the flukes is similar to engineered foils, which are classified by the National Advisory Committee for Aeronautics (NACA; Fish, 1998b). The NACA 63-021 foil (Abbott and von Doenhoff, 1949) provides a reasonable facsimile of the fluke sections (Fig. 8). Fluke profiles have also been compared with lesser known specialized airfoils, FX05-191 and EA6(-1-)-018 (Lang, 1966). The symmetrical profile of the NACA 0018 was used also to describe the cross-sectional fluke design of *Tursiops truncatus* (Kayan, 1979). The resemblance to the engineered NACA 63-021 foil suggests that the flukes would be able to produce high lift with low drag at angles of attack up to 17 degrees (Abbott and von Doenhoff, 1949). This would be possible because the shape of the fluke section does not promote extremes in the chordwise pressure distribution (Lang, 1966). Such extremes cause separation of flow from the foil surface, which induces stall and increases drag (Lang, 1966). At typical swimming speeds (2.5 m/sec and above) of dolphins, such as *Tursiops truncatus* (Williams et al., 1999; Fish and Rohr, 1999; Rohr et al., 2002), the maximum angle of attack is close to or below the 17 degrees stall angle for the NACA 63-021 foil (Fish, 1993). Indeed, angles of attack up to 30 degrees may be sustained by oscillating hydrofoils similar to dolphin flukes without stalling (Triantafyllou and Triantafyllou, 1995; Anderson et al., 1998). An oscillating foil can function at high angles of attack because of unsteady effects that enhance the pressure difference between the two sides of the foil and result in greater lift production.

For the various cetaceans from three odontocete families examined in this study, there is a consistency in the cross-sectional geometry. The cross-sectional geometry indicates similar hydrodynamic performance among cetaceans. With the exception of the single specimen of *Delphinus*, the cetaceans demonstrated high lift performance based on computational analysis (Fig. 7). *Lagenorhynchus* and *Delphinus* had the highest and lowest computed values of C_L, respectively. This finding was surprising as *Delphinus* is regarded as a high-speed swimmer (Hui, 1987). Compared with *Lagenorhynchus*, *Delphinus* has higher maximum swimming speeds (Table 2). Comparison of routine cruising speeds showed *Stenella* and *Tursiops* to have the highest speeds, whereas *Delphinus* cruises at low speeds commensurate with the lower value of C_L (Table 2). The variation of C_L and swimming speeds for cetaceans suggest that locomotor performance may be influenced by additional factors. Performance differences of cetacean flukes are expected due to scaling, material properties, kinematic control, and planform design.

Although the variation in cross-sectional geometry was low for species examined in this study, the planar geometry of flukes across the Cetacea does exhibit considerable variation, which can influence hydrodynamic performance (Fish, 1998b). The fluke shape approximates a delta wing with tapering tips with rearward sweep angle up to 47.4 degrees (Fish, 1998b). Tapered wings with sweepback have reduced drag with low stall characteristics (van Dam, 1987; Lee and Ho, 1990; Johansson and Norberg, 2003). Extreme departure from the general fluke shape is displayed by narwhals. The leading edge of the flukes of older males becomes slightly concave with no sweepback (Hay and Mansfield, 1989). Whether this fluke shape is a hydrodynamic adaptation associated with the unique, long tapering tusk exhibited by males, still remains to be investigated. Another interesting variant of fluke design is the crenelated trailing edge of the humpback whale. Tests on wings with serrated trailing edge indicate reduced drag (Bushnell and Moore, 1991), whereas a rippled trailing edge delays stall at the trailing edge and provides higher maximum lift (Werle et al., 1987).

CT scans provide an effective tool to collect high-resolution morphometric data on three-dimensional geometries. Interest in the development of biorobots and nonpropeller propulsive systems has focused on an examination of animal systems and locomotor performance (Triantafyllou and Triantafyllou, 1995; Taubes, 2000; Fish, 2006; Fish and Lauder, 2006). The paucity of detailed three-dimensional data on control surfaces has meant that engineers based predictive models and robotic designs on flat plates or standard foils. Such assumptions can limit performance capabilities (i.e., thrust production, lift generation, propulsive efficiency). Animal systems hold promise for improved performance by machines in the aquatic realm. The potential benefits from application of fluke geometry to manufactured systems operating in water are high speeds, vorticity control, energy economy, and enhanced maneuverability.

ACKNOWLEDGMENTS

We thank Julie Arruda, Perry Habecker, Scott Cramer, Jennifer Maresh, Mariela Muniz, Moira Nusbaum, and Robert Schoelkopf for their assistance. Flukes were collected with permission of the Northeast Regional Office of the National Marine Fisheries Service. This research was funded by a grant from the Office of Naval Research (Program manager Promode Bandyopadhyay).

LITERATURE CITED

Abbott I, von Doenhoff A. 1949. Theory of wing sections. New York: Dover.

Anderson J, Streitlien K, Barrett D, Triantafyllou M. 1998. Oscillating foils of high propulsive efficiency. J Fluid Mech 360:41–72.

Au D, Scott M, Perryman W. 1988. Leap-swim behavior of "porpoising" dolphins. Cetus 8:7–10.

Bose N, Lien J. 1989. Propulsion of a fin whale (*Balaenoptera physalus*): why the fin whale is a fast swimmer. Proc R Soc Lond B 237:175–200.

Bose N, Lien J, Ahia J. 1990. Measurements of the bodies and flukes of several cetacean species. Proc R Soc Lond B 242:163–173.

Bushnell D, Moore K. 1991. Drag reduction in nature. 23:65–79.

Cooper L, Berta A, Dawson S, Reidenberg JS. 2007. Evolution of hyperphalangy and digit reduction in the Cetacean manus. Anat Rec (this issue).

Cummings W, Thompson P, Cook R. 1968. Underwater sounds of migrating gray whales, *Eschrichtius glaucus* (Cope). J Acoust Soc Am 44:1278–1281.

Curren K, Bose N, Lien J. 1994. Swimming kinematics of a harbor porpoise (*Phocoena phocoena*) and an Atlantic white-sided dolphin (*Lagenorhynchus acutus*). Mar Mammal Sci 10:485–492.

Daniel T, Webb P. 1987. Physics, design, and locomotive performance. In: Dejours P, Bolis L, Taylor C, Weibel E, eds. Comparative physiology: Life in water and on land. New York: Springer-Verlag. p 343–369.

Felts W. 1966. Some functional and structural characteristics of cetacean flippers and flukes. In: Norris KS, editor. Whales, dolphins, and porpoises. Berkeley: University of California Press. p 255–276.

Fish F. 1993. Power output and propulsive efficiency of swimming bottlenose dolphins (*Tursiops truncatus*). J Exp Biol 185:179–193.

Fish F. 1998a. Comparative kinematics and hydrodynamics of odontocete cetaceans: morphological and ecological correlates with swimming performance. J Exp Biol 201:2867–2877.

Fish F. 1998b. Biomechanical perspective on the origin of cetacean flukes. In: Thewissen J, editor. The emergence of whales: evolutionary patterns in the origin of Cetacea. New York: Plenum Press. p 303–324.

Fish F. 2006. Limits of nature and advances of technology in marine systems: what does biomimetics have to offer aquatic robots? J Appl Bionics Biomech 3:49–60.

Fish F, Battle J. 1995. Hydrodynamic design of the humpback whale flipper. J Morphol 225:51–60.

Fish F, Rohr J. 1999. Review of dolphin hydrodynamics and swimming performance. SPAWARS Syst Cen Tech Rep 1801, San Diego, CA.

Fish F, Lauder G. 2006. Passive and active flow control by swimming fishes and mammals. Ann Rev Fluid Mech 38:193–224.

Gaskin D, Smith G, Watson A. 1975. Preliminary study of movements of harbour porpoises (*Phocoena phocoena*) in the Bay of Fundy using radiotelemetry. Can J Zool 53:1466–1471.

Hay K, Mansfield A. 1989. Narwhal *Monodon monoceros* Linnaeus, 1758. In: Ridgway SH, Harrison R, editors. Handbook of marine mammals. Vol. 4. San Diego: Academic Press. p 145–176.

Hoerner S. 1965. Fluid-dynamic drag. Published by author: Brick Town, NJ: Hoerner.

Howell A. 1930. Aquatic mammals. Springfield, IL: Charles C. Thomas.

Hui C. 1987. Power and speed of swimming dolphins. J Mammal 68:126–132.

Hurt H, Jr. 1965. Aerodynamics for naval aviators. US Navy, NAVWEPS 00-80T-80. Washington, DC: Department of the Navy.

Jacobs E, Ward K, Pinkerton R. 1933. The characteristics of 78 related airfoil sections from tests in the variable-density wind tunnel. NACA Rep. 460.

Johannessen C, Harder J. 1960. Sustained swimming speeds of dolphins. Science 132:1550–1551.

Johansson R, Norberg R. 2003. Delta-wing function of webbed feet gives hydrodynamic lift for swimming propulsion in birds. Nature 424:65–68.

Kayan V. 1979. The hydrodynamic characteristics of the caudal fin of the dolphin. Bionka 13:9–15. (translated from Russian).

Kruse S, Caldwell D, Caldwell M. 1999. Risso's dolphin *Grampus griseus* (G. Cuvier, 1812). In: Ridgway SH, Harrison R, editors. Handbook of marine mammals. Vol. 6. San Diego: Academic Press. p 183–212.

Lang T. 1966. Hydrodynamic analysis of dolphin fin profiles. Nature 209:1110–1111.

Lang T. Daybell D. 1963. Porpoise performance tests in a seawater tank. Nav Ord Test Sta Tech Rep 3063.

Lee M, Ho C-M. 1990. Lift force of delta wings. Appl Mech Rev 43:209–221.

Lighthill J. 1970. Aquatic animal propulsion of high hydromechanical efficiency. J Fluid Mech 44:265–301.

Lockyer C, Morris R. 1987. Observations on diving behaviour and swimming speeds in wild juvenile *Tursiops truncatus*. Aquat Mammal 13.1:31–35.

Mörzer Bruyns W. 1971. Field guide to whales and dolphins. Amsterdam: Mees.

Nowak R. 1991. Walker's mammals of the world. Baltimore: Johns Hopkins University Press.

Pavlov V. 2003. Wing design and morphology of the harbor porpoise dorsal fin. J Morphol 258:284–295.

Pilleri G, Knuckey J. 1969. Behaviour patterns of some Delphinidae observed in the western Mediterranean. Z Tierpsychologie 26:48–72.

Purves P. 1969. The structure of the flukes in relation to laminar flow in cetaceans. Zeit Saugertier 34:1–8.

Rohr J, Fish F, Gilpatrick J. 2002. Maximum swim speeds of captive and free ranging delphinids: critical analysis of extraordinary performance. Mar Mammal Sci 18:1–19.

Schultz W, Webb P. 2002. Power requirements of swimming: do new methods resolve old questions? Integ Comp Biol 42:1018–1025.

Shpet N. 1975. Distinctions of body shape and caudal fin of whales. Bionika 9:36–41.

Simpson G, Roe A, Lewontin R. 1960. Quantitative zoology. New York: Harcourt, Brace, Jovanovich.

Taubes G. 2000. Biologists and engineers create a new generation of robots that imitate life. Science 288:80–83.
Tomilin A. 1957. Mammals of the U.S.S.R. and adjacent countries. Vol. IX. Cetacea. Moscow: Nauk S.S.S.R. (English Translation, 1967, Israel Program for Scientific Translations, Jerusalem).
Triantafyllou G, Triantafyllou M. 1995. An efficient swimming machine. Sci Am 272:40–48.
van Dam C. 1987. Efficiency characteristics of crescent-shaped wings and caudal fins. Nature 325:435–437.
van Oossanen P, Oosterveld M. 1989. Hydrodynamic resistance characteristics of humans, dolphins and ship forms. Schiffstechnik 36:31–48.
Vogel S. 1981. Life in moving fluids. Boston: Willard Grant Press.
Vogel S. 1994. Life in moving fluids. Princeton: Princeton University Press.
von Mises R. 1945. Theory of flight. New York: Dover Publ.
Webb P. 1975. Hydrodynamics and energetics of fish propulsion. Bull Fish Res Bd Can 190:1–158.
Werle M, Paterson R, Presz M. 1987. Trailing edge separation/stall alleviation. AIAA J 25:624–626.
Williams T, Friedl W, Fong M, Yamada R, Sedivy P, Haun J. 1992. Travel at low energetic cost by swimming and wave-riding bottlenose dolphins. Nature 355:821–823.
Wood C. 1998. Movement of bottlenose dolphins around the southwest coast of Britain. J Zool 246:155–163.